

Micro-scale fracture experiments on zirconium hydrides and phase boundaries



H. Chan^{*}, S.G. Roberts, J. Gong

Department of Materials, University of Oxford, Parks Road, Oxford OX1 3PH, United Kingdom

ARTICLE INFO

Article history:

Received 3 November 2015

Received in revised form

24 March 2016

Accepted 29 March 2016

Available online 31 March 2016

ABSTRACT

Fracture properties of micro-scale zirconium hydrides and phase boundaries were studied using microcantilever testing methods. FIB-machined microcantilevers were milled on cross-sectional surfaces of hydrided samples, with the most highly-stressed regions within the δ -hydride film, within the α -Zr or along the Zr-hydride interface. Cantilevers were notched using the FIB and then tested in bending using a nanoindenter. Load-displacement results show that three types of cantilevers have distinct deformation properties. Zr cantilevers deformed plastically. Hydride cantilevers fractured after a small amount of plastic flow; the fracture toughness of the δ -hydride was found to be $3.3 \pm 0.4 \text{ MPam}^{1/2}$ and SEM examination showed transgranular cleavage on the fracture surfaces. Cantilevers notched at the Zr-hydride interface developed interfacial voids during loading, at loads considerably lower than that which initiate brittle fracture of hydrides.

© 2016 Published by Elsevier B.V.

1. Introduction

Zirconium alloys are widely used as nuclear fuel cladding materials mainly because of their low neutron absorption cross-section; however hydrogen formed as a product of waterside corrosion can lead to embrittlement [1]. Hydrogen diffuses into the claddings to form polycrystalline zirconium hydrides when the concentration exceeds the solubility limit. A considerable drop in ductility has been observed in room temperature mechanical tests carried out for samples with compositions where the face-centred cubic δ -phase hydride is dominant [2–4]. The local stress which initiates the brittle fracture of hydride precipitates is a key input parameter to models of delayed hydride cracking (DHC) [5–7]. Fracture toughness measurements on 3.5 mm thick compact tension Zr hydride specimens obtained a value of about $1 \text{ MPam}^{1/2}$ and transgranular cleavage was observed on the δ -hydride fracture surfaces [8]. However, these tests are on large-scale “bulk” hydrides, rather than the micron to ~100 micron-scale precipitates involved in DHC. Direct loading tests on micro-scale crack-free hydrides should provide data more applicable to investigating DHC behaviour.

Methods developed for micromechanical testing on thin films

and miniaturized devices can be applied to investigate the fracture behaviour of Zr hydrides [9]. Nanoindentation can allow fracture toughness determination by measuring crack lengths generated during controlled indentation. However Schiffmann [10] demonstrated that the results differed from literature values in a study testing a number of different bulk and thin film materials. The main source of error probably came from the difference between the true crack geometries and the assumptions of the models used to derive fracture toughness; the configurations of the cracks present around the indenter differed considerably from the ideal crack types. The poor accuracy of fracture toughness determined from these complex three dimensional crack system with substantial deformation residual stresses was also discussed by Quinn and Bradt [11]. Also, in the testing of small precipitates, the viable maximum indentation load may be insufficient to generate any fracture; it would be below the critical load P^* identified by Lawn and Evans [12], typically a few tens of mN for hard and brittle materials.

Other applicable methods involve fracture test specimens being prepared on a selected local area by micro-machining techniques such as focused ion beam (FIB), photolithography or plasma etching. A variety of geometries including pillars [13,14], clamped beams [15], cantilevers [16–20] and double cantilevers [21] have been used to carry out microfracture tests [22]. In all geometries, controlled direct loads are applied on the specimens by using a nanoindenter to introduce displacement until fracture occurs.

^{*} Corresponding author.

E-mail address: howard.chan@materials.ox.ac.uk (H. Chan).

Finite element method (FEM) is usually used to analyse data in order to determine the stress intensity factor and the fracture toughness. In the case of testing fracture properties of Zr hydrides by pillars and double cantilevers, the friction coefficient between the indenter tip and the sample can influence the results and its value is largely unknown. Clamped beams are capable of supporting stable crack growth however the residual stress may influence the fracture process [22]. Single cantilevers allow post-examination of the fracture surfaces and measurement of fracture toughness at chosen locations in order to investigate the micro-structural properties of anisotropic materials and interfaces. The method has been demonstrated to be effective in studying a range of materials such as silicon [16], silicon based passivation films [17], bismuth embrittled copper grain boundaries [18], anisotropic NiAl [19] and semi-brittle tungsten [20].

In the present study, in order to investigate the fracture behaviour of the δ -hydride and its interface with the α -Zr matrix, FIB-machined pre-cracked cantilevers were deflected using a nanoindenter at room temperature. The results were compared with the testing of non-hydrided α -Zr cantilevers of the same dimensions. SEM and EBSD were used to examine the microstructure and the fracture surfaces.

2. Experimental

2.1. Materials and preparation

A commercial grade unalloyed 99.2% Zr rod (Goodfellow Metals, Cambridge Ltd.) was annealed for 72-h at 750 °C and then cut into 10 mm × 7.5 mm × 1 mm samples. The 7.5 mm × 1 mm surface, which was used for preparing microcantilevers, had the normal direction parallel to the radial direction of the rod. The average grain diameter was approximately 70 μ m. More details on the texture and the grain structure are described elsewhere [23]. The large surface (charging surface) was ground using 120–4000 grit SiC paper and mechanically polished for 24 h using colloidal silica. An electrochemical technique was used to produce a hydride film. The sample was spot welded to a Zr wire and then immersed in 0.5%vol sulphuric acid electrolyte to form a cathode. The back and side surfaces were covered with lacquer and the remaining charging surface was positioned parallel to a platinum mesh anode at a distance of about 30 mm. The hydriding process operated at 65 °C under a supply current density of 1.5 kA/m² for durations ranging from 12 to 130 h.

Each charged sample was then cut using a low speed saw for examination of the charging surface and the 7.5 mm × 1 mm cross-sectional surface. All microstructural examinations were located at least 3 mm away from the welding spot. The cross-sectional samples were covered by a thin layer of silver conductive paint before being embedded in resin. After grinding and polishing, the final cross-sectional surface was etched by a solution of 1%vol HF, 10% HNO₃ and 89% H₂O for 20 s.

2.2. Microstructure

The charging surface and the cross-sectional surface of the samples hydrided for various durations were examined using polarised light microscopy and SEM. Hydride islands of ~5 μ m in diameter formed on the charging surface in the first 30 min. Their diameter increased to 10 μ m after 12 h (Fig. 1a). The number of islands increased with the charging time and eventually connected to form a continuous hydride film (Fig. 1b–d). Sub-surface micro-scale cracks, roughly parallel to the charging surface, were observed within the hydride film in all samples (Fig. 1d). This crack formation does not result from the cross-sectioning or polishing process since

cracks of similar dimensions were also seen inside the film after FIB milling.

Fig. 1e shows an example of a lens-shaped δ -hydride island on a cross-sectional foil. The crystallographic orientation relationship of the two phases was identified as $\{0001\}_{\alpha} \parallel \{111\}_{\delta}$ by EBSD. Hydride precipitates of 0.2–1 μ m long and 0.03–0.1 μ m thick measured directly from the image are closely stacked and aligned near the continuous phase boundary. Fig. 1f indicates that the orientation of hydride precipitates changes across a Zr grain boundary.

2.3. Micromechanical testing

All micromechanical tests were carried out on the cross-sectional samples near the charging edge (Fig. 2). Microstructures were examined under polarised light and using scanning electron microscopes, followed by EBSD phase identification. Cantilevers were made on cross-sectional surfaces (a) wholly within the hydride; (b) wholly within the α -Zr; and (c) having the pre-crack on the Zr-hydride interface with the fixed end of the cantilever in the hydride phase. In order to ensure positional accuracy, location marks were made by nanoindentation several tens of microns away from the planned positions prior to micromachining. The typical positions and the dimensions of the pentagonal cantilevers are illustrated in Fig. 2. All cantilevers and the T-shaped dimension calibration marks were fabricated using 30 keV Ga⁺ ions in an FEI FIB200. The FIB milling procedures are described in detail in the work of Di Maio and Roberts [16]. The use of the pentagonal cross-section allows milling of cantilevers at selected locations anywhere on the sample surface, rather than being restricted working at sample edges. A scanning current of 100 pA was used in the final cantilever milling step to produce sharp edges and corners. The notch and the crack tip were then produced by single passes of the Ga beam at 10 pA and then 1 pA. Each cantilever was tilted at 0°, 30° and 45° for dimensional measurements.

The pre-cracked microcantilevers were tested in an Agilent Nano Indenter G200-XP using a Berkovich tip. A topographical map of the T-shaped mark was produced in scanning mode for the purpose of setting up a reference position and a surface height. The indenter tip was then moved along the longitudinal centre-line to the loading position which was 9 μ m away from the fixed end. The deflection test was carried out at a displacement rate of 5 nm/s until a sharp load drop occurred or to a maximum preset displacement of 2 μ m. After the tests, all cantilevers were tilted at the same angles and re-imaged as for the initial dimensional measurements (Fig. 4a and b). Where possible, the dimensions of cantilevers were re-measured on fracture surfaces (Fig. 4d).

3. Results

3.1. Fracture behaviour of hydrides, Zr and interfaces

The distinct deformation properties of the different types of cantilevers are compared in the load-displacement curves as shown in Fig. 3. The hydride cantilevers yielded slightly before a sudden failure occurred at a deflection of about 1000 nm. The Zr cantilevers continued to undergo plastic deformation without a sharp load drop until the preset displacement limit of 2000 nm. The load at which hydrides start to yield is clearly higher than that of Zr. The interface-notched cantilevers deformed similarly to the Zr cantilevers but then fractured in the plastic deformation region. The slope of the elastic region of all curves is apparently very similar.

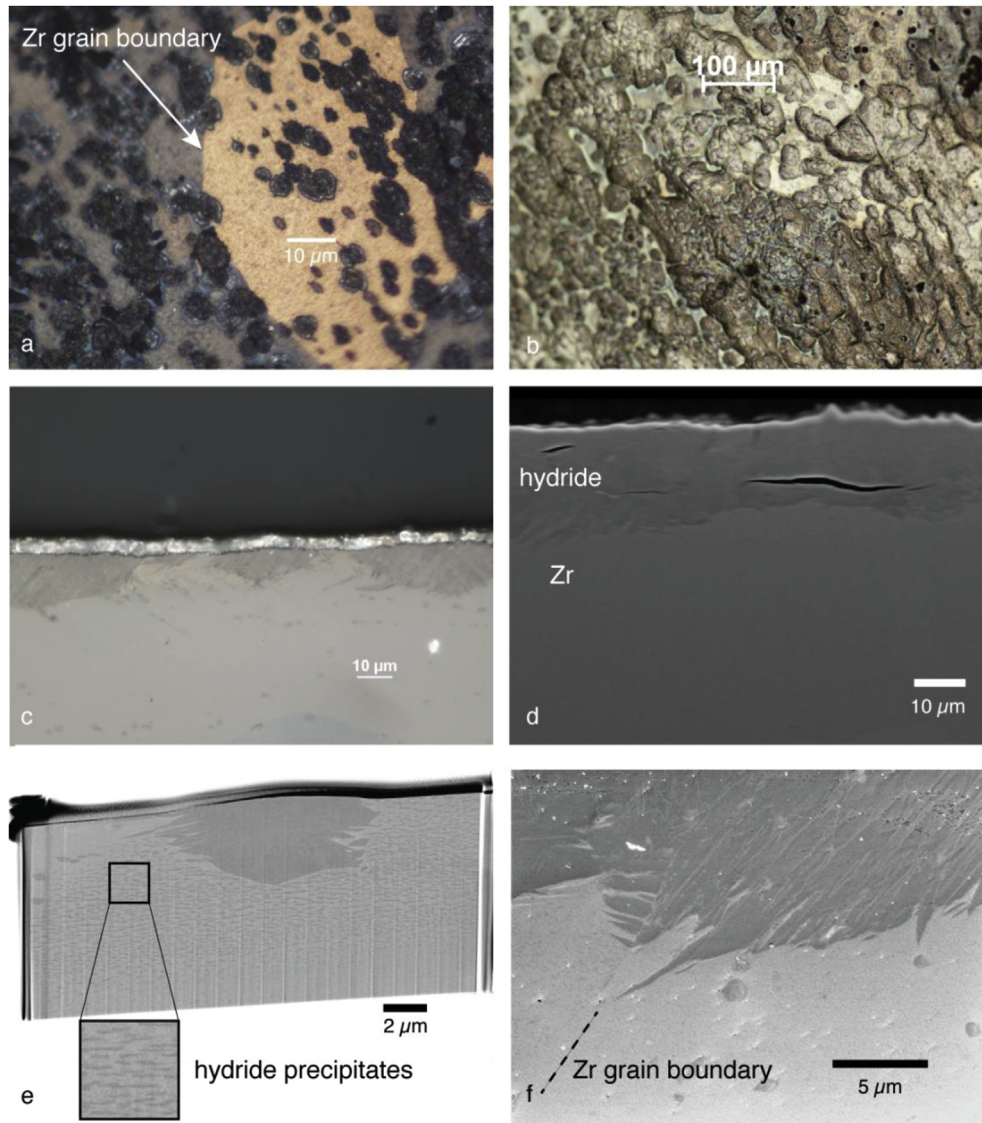


Fig. 1. Microstructure of Zr hydride films. a) Hydride islands formed on the charging surface after 12 h; and b) 130 h c) Isolated hydride islands were observed on the cross-sectional surface of a 16-h charged sample. d) Islands connected to form a continuous film after 96 h of hydrogen charging. Micro-cracks were seen on all hydride films. e) Closely stacked hydride precipitates align near a lens-shaped island on a cross-sectional foil. f) The orientation of hydride precipitates changes across a Zr grain boundary.

3.2. Fracture surfaces

Fig. 4a and b shows an example of a pre- and post-test hydride cantilever. Most of the hydride cantilevers separated into two pieces after loading, and the propagated crack can be seen on material still attached to the fixed end (Fig. 4c). Transgranular cleavage associated with ridges was seen on the non-smooth brittle fracture surfaces in Fig. 4d. The Zr cantilevers showed plastic deformation and slip lines near the fixed end, without apparent surface opening of the pre-crack (Fig. 5). The absence of fracture is consistent with the load-displacement test results shown in Fig. 3. The size of the indenter tip mark at the loading position is larger than that on the hydride cantilevers because of the lower hardness of Zr. For the interface-notched cantilevers, voids of diameter roughly 200 nm formed along the interface prior to crack propagation, as shown in Fig. 6. Such voids were not seen in either the Zr or the hydride cantilevers. The load-displacement curves (Fig. 3) imply that the load needed to form voids and separate the hard hydride precipitates from the Zr matrix is considerably lower than

that which initiates brittle fracture of hydrides.

3.3. Fracture toughness of hydrides

For an initial analysis of the load-displacement data, the δ -hydride is assumed to be a linear elastic material, as an approximation to the blue curves in Fig. 3. Fracture toughness values K_{IC} were calculated using linear elastic fracture mechanics (LEFM), as in the micromechanical fracture work of Di Maio and Roberts [16] and Matoy et al. [17],

$$K_{IC} = \sigma_0 \sqrt{\pi a} F\left(\frac{a}{2\bar{y}}\right) \quad (1)$$

$$\sigma_0 = \frac{P_0 L_0 \bar{y}}{I} \quad (2)$$

where a is the pre-crack length and \bar{y} is the vertical distance between the upper surface and the centroid of the cross-section. P_0 is

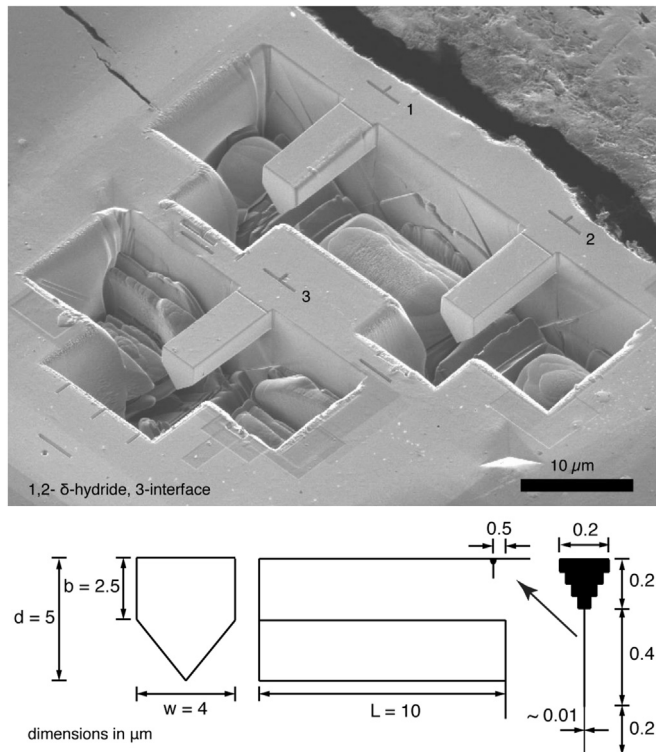


Fig. 2. The δ -hydride (1 and 2) and the phase boundary interface-notched (3) microcantilevers fabricated on the cross-section of a hydride film and their typical dimensions in μm . The SEM image shows the 45° tilted surface. Nanoindentation location marks were made at several tens of microns away from the planned interface position prior to FIB machining. Naturally formed cracks were observed near the charging edge as seen in the upper left corner of the SEM image.

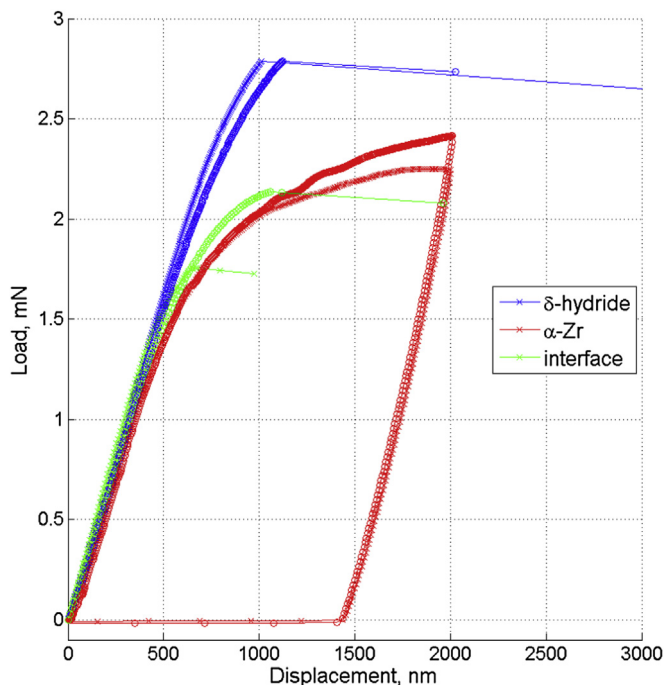


Fig. 3. Typical load-displacement curves of micro-scale pre-cracked cantilevers tested at room temperature. The hydride cantilevers slightly yielded before fracture occurred. The average fracture load of the hydride cantilevers is significantly higher than that of the interface-notched cantilevers. The Zr cantilevers deformed without fracture until a preset displacement limit of $2 \mu\text{m}$.

the fracture load, L_0 is the longitudinal distance between the pre-crack and the indenter tip loading point and I is the second moment of area. For the pentagonal cross-section shape illustrated in Fig. 2 where b is half of the total depth, $\bar{y} = 7b/9$ and $I = 999w \bar{y}^3/1372$.

The dimensionless shape factor $F(a/2\bar{y})$ was determined by finite element analysis using ABAQUS. Three-dimensional quadratic elements and isotropic material properties were used to create pentagonal cantilever models. An encasté boundary condition was assigned to the bottom, the back and the side surfaces of a block attached to the cantilever (Fig. 7). The simulation was then performed by applying a downward displacement along the width near the free end. Contour integrals surrounding the crack front and the free end reaction forces were computed for various crack lengths. Convergence studies were carried out to optimise the mesh sizes and the output number of contours. The cubic polynomial fitting equation of the factor F is shown in Fig. 7. The factor was then substituted into Eq. (1) to determine K_{IC} . In the present microfracture experiments, typical values are $a/2\bar{y} = 0.21$ and $F = 1.03$.

The dimensionless shape factors provided in various research studies are plotted against $a/2\bar{y}$ in Fig. 7. All the factors were deduced from finite element models for isotropic elastic materials based on LEFM. A main difference between the models is the designed cross-sectional shape of the cantilevers. Rectangular cantilevers were used in the work of Matoy et al. [17], Iqbal et al. [19], and Wurster, Motz and Pippan [20] and pentagonal cantilevers were used in the others. The factor obtained in the work of Di Maio and Roberts [16] is noticeably higher than the others. The maximum percentage difference from the mean of those factors is 5.1% in the range $0.2 \leq a/2\bar{y} \leq 0.5$. Tests were carried out on six hydride cantilevers and their fracture toughness was found to be $3.3 \pm 0.4 \text{ MPa m}^{1/2}$. The error range given is the standard deviation in calculated fracture toughness and it results from the scatter in the measurements rather than from any variability in the calculated dimensionless shape factor F .

3.4. Mechanical properties

The deformation behaviour of the cantilevers was studied through a multiple loading and imaging method. A cantilever was first loaded slightly above the limit of proportionality, and then examined by SEM. It was loaded again to generate more plastic deformation and the procedure repeated. Fig. 8 shows the results for an interface-notched cantilever. The specimen shows only plasticity up to a sudden fracture at the maximum load. Crack initiation occurred only after the first two cycles of loading (Fig. 8b–d). This indicates that the load-displacement curve at loads below the maximum value relates to the plastic deformation of the cantilever alone, rather than to any crack opening or extension. The yield and flow behaviour can therefore be modelled independently of fracture behaviour using these first two loading cycles.

For the analysis of the pre-fracture portion on the load-displacement data, plastic properties were specified in the FE model described in Section 3.3 to compute the yield strength of both materials. The method was modified from MATLAB codes written for analysing the plastic deformation of non-cracked microcantilevers [24]. An experimental curve was first divided into five segments; the first one being the linear-elastic portion. The simulations of load-displacement were then fitted to the segmental experimental curve via a process of progressive convergent approximation by adjusting the model material's properties. The iterative process was repeated until all the simulated loads were within 1% of the experimental loads. Table 1 shows

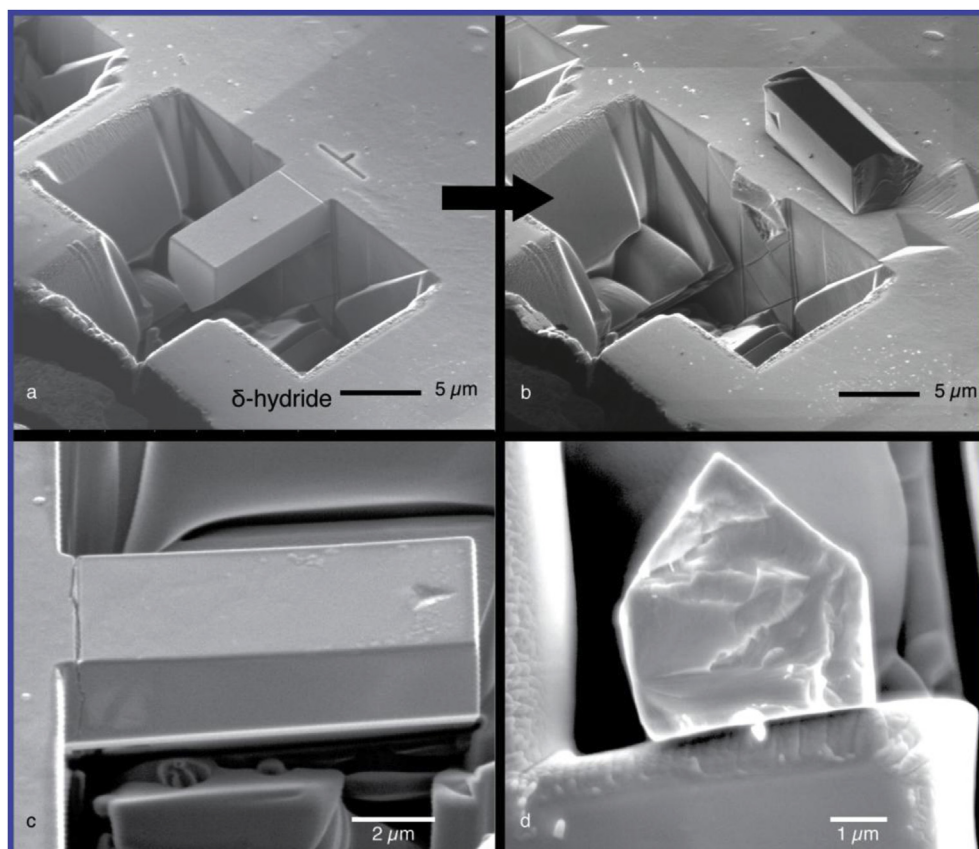


Fig. 4. SEM examination of the fractured δ -hydride microcantilevers. a and b) Samples were tilted at the same angle after the deflection test for comparison. Non-smooth fracture surfaces were initiated from the pre-crack. c) Side view of a tested hydride cantilever shows the propagated crack. d) Transgranular cleavage on the hydride fracture surface. The dimensions of the cross-section were re-measured for this cantilever.

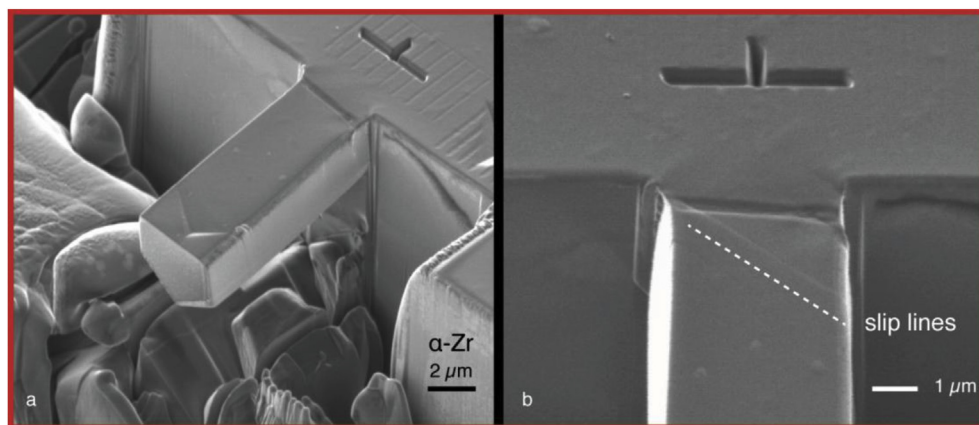


Fig. 5. The ductile α -Zr cantilevers deformed plastically without fracture. Slip lines were seen on some specimens near the fixed end.

the results for the Zr and the hydride pre-cracked cantilevers. The FE model for the interface-notched cantilevers was built by assigning two sections consisted of the corresponding model materials; here, the simulations of load-displacement were also within the predefined 1% accuracy.

4. Discussion

The microfracture tests show that the δ -hydride phase is relatively brittle, with $K_{IC} = 3.3 \pm 0.4 \text{ MPam}^{1/2}$. This value was

determined from single phase specimens which did not contain naturally formed micro-cracks. It is higher than the macroscopic measurement of about $1 \text{ MPam}^{1/2}$ obtained from testing bulk Zr hydride samples [8]. This higher toughness value may be related to the observation that the δ -hydride is not completely brittle on this small scale, as indicated by a slight curvature of the lines before fracture in Fig. 3. This is possibly due to deformation at the notch or crack tip produced by the high local shear stresses.

Young's moduli determined for both phases are in good agreement with literature values as shown in Table 1. Higher yield

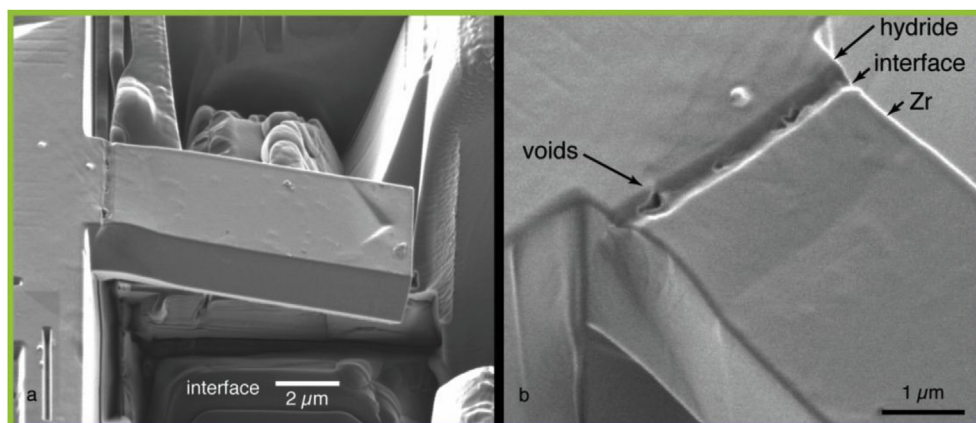


Fig. 6. An interface-notched cantilever with the fixed end being in the δ -hydride. Plastic deformation associated with slip lines can be seen on the α -Zr surface. Voids of diameter ~ 200 nm were observed along the interface.

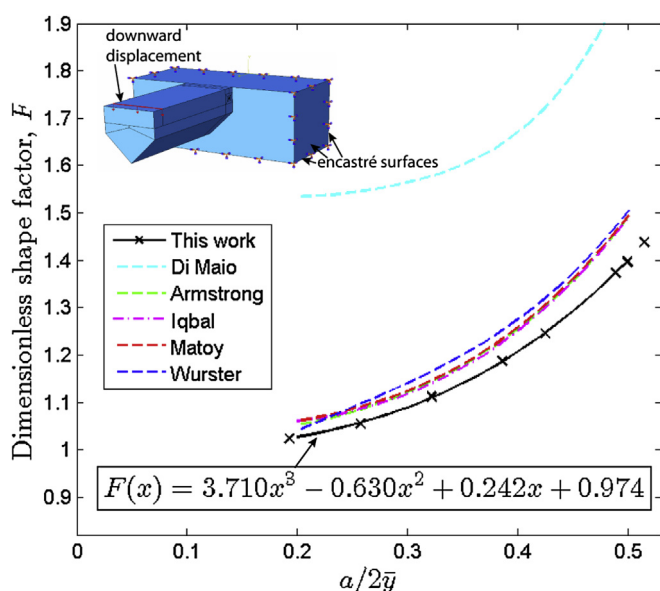


Fig. 7. Three-dimensional finite element model for calculating the dimensionless shape factor F . The J-integral was computed for various crack lengths, a , to determine the value of fracture toughness. \bar{y} is the distance between the upper surface and the centroid of the cross-section. The cubic polynomial fitting curve of F is plotted in black. Dashed curves are generated from equations provided in the studies [16–20]. The microcantilevers used in these studies vary in dimensions and shapes.

strengths are obtained in our microcantilever tests compared to those found in larger-scale test. Such size effects are well known in many materials, with yield stresses increasing markedly with decreasing specimen size, especially for specimen sizes below $\sim 10 \mu\text{m}$ [20]. The yield stress values found in the current study are consistent with those from micro-scale pillar test results for Zircaloy (530 MPa) and for hydrided specimens (900–1600 MPa) [27].

The properties of the interface differ from those of the individual phases. Voids formed at the interface at a relatively low stress, prior to eventual interface failure (Figs. 6b and 8f). Although void growth and coalescence upon further loading can lead to intergranular rupture and separation of the hard hydrides from the Zr matrix, the amount of strain energy released may exceed the critical value for fracture of the associated hydrides. In the experimental arrangement used here, one interface-notched cantilever cracked in the hydride fixed end instead of from the pre-crack. During the SEM in-

situ macroscopic tensile test of bulk Zr hydride carried out by Arsene, Bai and Bompard [4], cracks always appeared inside the hydrides and no fracture of the interface was observed. In another in-situ examination of macroscopic crack growth in polycrystalline Zr hydrides [28], both transgranular and intergranular crack paths associated with fractured hydride precipitates were observed; the type of fracture was influenced by the orientation of hydride precipitates relative to the crack tip. The type of fracture in a particular hydride-rich microstructure is likely to be dependent on the complex three-dimensional stress states near the crack.

5. Summary

In this paper we report results on the microfracture cantilever experiments on the Zr hydride film and its interface with the α -Zr matrix. The main findings are:

1. Hydrogen diffuses into the Zr sample surface to form micro-scale lens-shaped hydride islands. $0.2\text{--}1 \mu\text{m}$ long hydride precipitates are closely stacked and aligned near the phase boundary.
2. The δ -hydride, the α -Zr and the Zr-hydride interface have distinct deformation properties. The hydrides yielded slightly at 1160–1390 MPa before brittle fracture occurred while the ductile α -Zr deformed plastically. The interface-notched cantilevers fractured after moderate plastic deformation.
3. The fracture toughness of the δ -hydride was measured to be $3.3 \pm 0.4 \text{ MPa}\sqrt{\text{m}}$. The fracture surfaces showed mostly transgranular cleavage with some ridges.
4. For the specimens notched along the interface, voids formed by opening of the Zr-hydride interface. The average load needed to form voids and separate the hard hydride precipitates from the Zr matrix is lower than that which initiates brittle fracture of hydrides.

This study demonstrates that precision microcantilever testing methods are capable of measuring local and interfacial mechanical properties within a dual-phase zirconium/zirconium hydride microstructure. Further study using these methods could help develop a better understanding of the relationships between local plasticity and fracture initiation and propagation in these materials, contributing to improved models of zirconium alloy performance in hydriding environments.

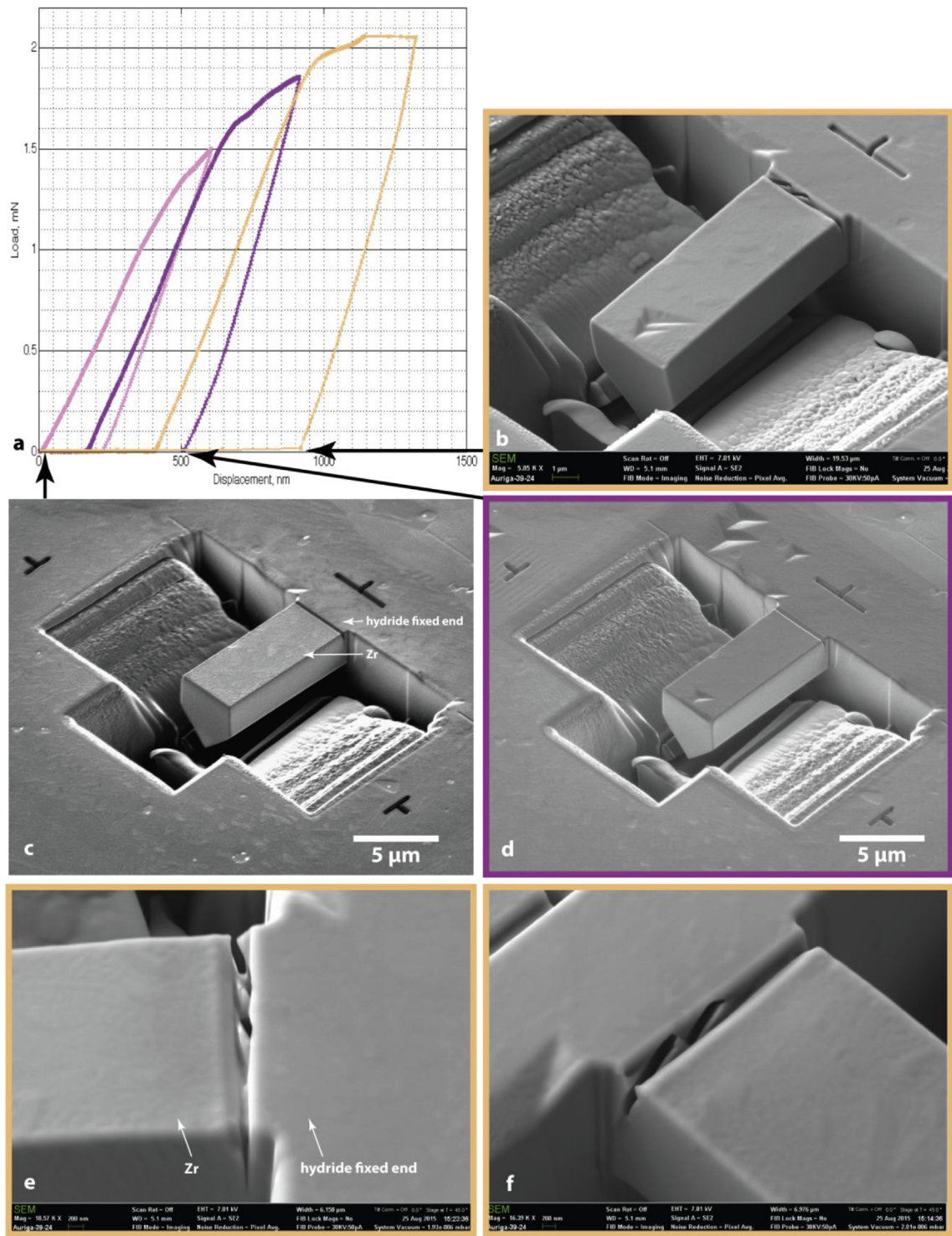


Fig. 8. Multiple loading and imaging on an interface-notched cantilever. a) The specimen was loaded three times; a load drop was observed only in the last cycle. b) Post examination of the fractured specimen. c) and d) No crack initiation was observed in the specimen when loaded to below 1000 nm displacement. e) and f) Hydrides detached from the Zr matrix along the phase boundary after the third cycle.

Table 1
Micromechanical properties determined for the pre-cracked microcantilevers in comparison with literature results.

	α -Zr: this study	α -Zr alloys: literature data [5,23,25]	δ -Hydride: this study	Hydrided Zr alloys: literature data [3–5,26]
Young's modulus (GPa)	80–85	82.2–100	78–82	80–95
Yield strength (MPa)	570–680	205–540	1160–1390	600–800

Acknowledgements

The authors gratefully acknowledge the help of Hannah Weekes (Imperial College) in the preparation of hydrided samples. The study was part-funded by EPSRC grant EP/I003274/1.

References

- [1] D.O. Northwood, U. Kosasih, Hydrides and delayed hydrogen cracking in zirconium and its alloys, *Int. Metals Rev.* 28 (2) (1983) 92–121.
- [2] K.G. Barraclough, C.J. Beevers, Some observations on the deformation characteristics of bulk polycrystalline zirconium hydrides. Part 1: the deformation and fracture of hydrides based on the δ -phase, *J. Mater. Sci.* 4 (6) (1969) 518–525.
- [3] M.P. Puls, S.-Q. Shi, J. Rabier, Experimental studies of mechanical properties of solid zirconium hydrides, *J. Nucl. Mater.* 336 (1) (2005) 73–80.
- [4] S. Arsene, J. Bai, P. Bompard, Hydride embrittlement and irradiation effects on the hoop mechanical properties of pressurized water reactor (PWR) and boiling-water reactor (BWR) Zircaloy cladding tubes: Part III, *Metall. Mater. Trans. A* 34 (3) (2003) 579–588.
- [5] S.-Q. Shi, M.P. Puls, Criteria for fracture initiation at hydrides in zirconium alloys I. Sharp crack tip, *J. Nucl. Mater.* 208 (3) (1994) 232–242.
- [6] E. Darby, M. Martin, D. Scarth, Delayed hydride cracking in zirconium alloys – a review of mechanisms, assessment criteria and current developments, in: TAGSI/FESI Symposium Structural Integrity of Nuclear Power Plant, 2013, pp. 1–19.
- [7] T. Kubo, Y. Kobayashi, Effects of δ -hydride precipitation at a crack tip on crack propagation in delayed hydride cracking of Zircaloy-2, *J. Nucl. Mater.* 439 (1–3) (2013) 202–211.
- [8] L.A. Simpson, C.D. Cann, Fracture toughness of zirconium hydride and its influence on the crack resistance of zirconium alloys, *J. Nucl. Mater.* 87 (2–3) (1979) 303–316.
- [9] S. Zhang, D. Sun, Y. Fu, H. Du, Toughness measurement of thin films: a critical review, *Surf. Coat. Technol.* 198 (1–3) (Aug. 2005) 74–84.
- [10] K.I. Schiffmann, Determination of fracture toughness of bulk materials and thin films by nanoindentation: comparison of different models, *Philos. Mag.* 91 (7–9) (2011) 1163–1178.
- [11] G.D. Quinn, R.C. Bradt, On the Vickers indentation fracture toughness test, *J. Am. Ceram. Soc.* 90 (3) (2007) 673–680.
- [12] B.R. Lawn, A.G. Evans, A model for crack initiation in elastic/plastic indentation fields, *J. Mater. Sci.* 12 (1977) 2195–2199.
- [13] B. Moser, K. Wasmer, L. Barbieri, J. Michler, Strength and fracture of Si micropillars: a new scanning electron microscopy-based micro-compression test, *J. Mater. Res.* 22 (4) (2007) 1004–1011.
- [14] M. Sebastiani, K.E. Johanns, E.G. Herbert, F. Carassiti, G.M. Pharr, A novel pillar indentation splitting test for measuring fracture toughness of thin ceramic coatings, *Philos. Mag.* 95 (16–18) (2015) 1928–1944.
- [15] B.N. Jaya, V. Jayaram, S.K. Biswas, A new method for fracture toughness determination of graded (Pt,Ni)Al bond coats by microbeam bend tests, *Philos. Mag.* 92 (25–27) (2012) 3326–3345.
- [16] D. Di Maio, S.G. Roberts, Measuring fracture toughness of coatings using focused-ion-beam-machined microbeams, *J. Mater. Res.* 20 (2) (2005) 299–302.
- [17] K. Matoy, H. Schönherr, T. Detzel, T. Schöberl, R. Pippan, C. Motz, G. Dehm, A comparative micro-cantilever study of the mechanical behavior of silicon based passivation films, *Thin Solid Films* 518 (1) (Nov. 2009) 247–256.
- [18] D.E.J. Armstrong, A. Wilkinson, S.G. Roberts, Micro-mechanical measurements of fracture toughness of bismuth embrittled copper grain boundaries, *Philos. Mag. Lett.* 91 (6) (2011) 394–400.
- [19] F. Iqbal, J. Ast, M. Göken, K. Durst, In situ micro-cantilever tests to study fracture properties of NiAl single crystals, *Acta Mater.* 60 (3) (2012) 1193–1200.
- [20] S. Wurster, C. Motz, R. Pippan, Characterization of the fracture toughness of micro-sized tungsten single crystal notched specimens, *Philos. Mag.* 92 (14) (May 2012) 1803–1825.
- [21] S. Liu, J.M. Wheeler, P.R. Howie, X.T. Zeng, J. Michler, J. Clegg, Measuring the fracture resistance of hard coatings, *Appl. Phys. Lett.* 102 (2013), 171907–1–4.
- [22] B.N. Jaya, C. Kirchlechner, G. Dehm, Can microscale fracture tests provide reliable fracture toughness values? A case study in silicon, *J. Mater. Res.* 30 (5) (2015) 686–698.
- [23] J. Gong, T.B. Britton, M.A. Cuddihy, F.P.E. Dunne, A.J. Wilkinson, (a)Prismatic, (a)basal, and (c+a) slip strengths of commercially pure Zr by micro-cantilever tests, *Acta Mater.* 96 (Sep. 2015) 249–257.
- [24] C.D. Hardie, Micro-mechanics of Irradiated Fe-Cr Alloys for Fusion Reactors, DPhil, University of Oxford, 2013.
- [25] D.O. Northwood, The development and applications of zirconium alloys, *Mater. Des.* 6 (2) (1985) 58–70.
- [26] S.-Q. Shi, M.P. Puls, Fracture strength of hydride precipitates in Zr-2.5Nb alloys, *J. Nucl. Mater.* 275 (3) (1999) 312–317.
- [27] H.E. Weekes, V.A. Vorontsov, I.P. Dolbnya, J.D. Plummer, F. Giuliani, T.B. Britton, D. Dye, In situ micropillar deformation of hydrides in Zircaloy-4, *Acta Mater.* 92 (2015) 81–96.
- [28] G. Bertolino, G. Meyer, J. Perez Ipiña, In situ crack growth observation and fracture toughness measurement of hydrogen charged Zircaloy-4, *J. Nucl. Mater.* 322 (1) (2003) 57–65.